Available online at www.sciencedirect.com
SCIENCE DIRECT®
International Journal of Mass Spectrometry 226 (2003) 291–304
International Journal of Mass Spectrometry
www.elsevier.com/locate/ijms

Photodissociation spectroscopy of Mg^+–pyridine complex

Wenyue Guo[a,b,*], Haichuan Liu[a], Shihe Yang[a,1]

[a] *Department of Chemistry, The Hong Kong University of Science and Technology, Clear Water Bay, Kowloon, Hong Kong*
[b] *Applied Physics Department, University of Petroleum, China Dongying, Shandong 257061, PR China*

Received 8 December 2002; accepted 15 January 2003

Abstract

Photodissociation spectroscopy of the Mg^+–pyridine complex in the spectral range of 240–440 nm is presented in the paper. Mass spectrometry of the complex exhibits the persistent product Mg^+ from non-reactive quenching throughout the whole wavelength range. A minor charge transfer (CT) product $C_5H_5N^+$ is also observed when the laser wavelength is shorter than 249 nm. The action spectrum of the complex was recorded as a function of laser wavelength. Three pronounced bands with a symmetrical feature were observed in the action spectrum. The optimized geometry of Mg^+–pyridine is characterized by the linkage of Mg^+ to the N atom of the molecule possessing a C_{2v} symmetry with Mg on the C_2 axis of the complex. The calculated vertical absorption spectrum of the complex using the optimized structure of its ground state agrees qualitatively with the observed action spectrum. The relative yield of the CT product shows a threshold feature and rises with the shortening of the laser wavelength. The action spectrum of the CT product has a nearly similar feature to that of the total ion in the wavelength range of 240–250 nm. Based on the experimental results, the predissociative CT reaction mechanism is invoked to account for the yield of the photoinduced CT product $C_5H_5N^+$.

Keywords: Mg^+–pyridine complex; Photodissociation spectroscopy; Charge transfer

1. Introduction

Photodissociation of metal cation–molecular 'precursor' complexes often gives valuable information about the complex structures and the intermolecular interactions [1–7]. It has also been proven to be an effective way to probe bond strengths of ion species [8,9]. Many experimental [1–7,10–17] and theoretical [18–22] studies of metal cation–molecular complexes involved singly charged alkaline earth metal cations because they have an open-shell 'radical' structure with their intense atomic resonances ($^2P \leftarrow {}^2S$) easily accessed by visible and ultraviolet light. Our group has reported a number of intra-complex reactions, such as C–F [23–26], C–O [26], C–N [27–29], and N–H [28,29] bond excitations and charge transfer (CT), by the use of a photon and an appropriate metal cation–molecule complex. These reactions not only reveal the interactions of the metal cation and the

* Corresponding author. Tel.: +86-546-8391122; fax: +86-546-7366374.
E-mail addresses: wyguo@mail.hdpu.edu.cn (W. Guo), chsyang@ust.hk (S. Yang).
[1] Co-corresponding author.

1387-3806/03/$ – see front matter © 2003 Elsevier Science B.V. All rights reserved.
doi:10.1016/S1387-3806(03)00020-4

molecules, which are very important in a wide range of biological, cosmochemical, environmental, chemical, and physical processes, but also open a window for the isolation, characterization, and investigation of the chemical reactivity of some interesting radical cations [25].

Pyridine is one of the most abundant and best known of aromatic heterocyclics. Compounds containing the pyridine ring are widely distributed in nature, principally as enzymes and alkaloids. Pyridine enzymes have been found in the tissues of all plants and animals examined thus far, and are derived from either nicotinic acid or Vitamin B_6 [30]. Pyridine is also the building block of many pharmaceuticals with a wide range of functionalities that include anti-tubercular compounds, antiviral and antitumor agents, central nervous system stimulants, diagnostic agents, analgesics, anti-inflammatory agents, and antihistamines [31,32]. On the other hand, metal cations are involved in all biological processes that nucleic acids participate in. The effects of binding a metal cation to a nucleic acid vary from stabilization of the three-dimensional structure to transfer failure and even cell death. Pyridine is often chosen as a simple model of non-covalent interaction with metal cations for a wide variety of nitrogen-containing heterocyclics of biological importance, and of particular interest, the nucleic acid bases.

Much attention has been paid to the interactions and photoinduced reactions of M^+–pyridine. Rodgers et al. [33,34] have studied the periodic trends in the binding of M^+–pyridine (M = Mg, Al, Sc, Ti, V, Cr, Mn, Fe, Co, Ni, and Zn; Li, Na, and K) based on threshold collision-induced dissociation and density functional theory. Photoinduced CT reactions of M^+–pyridine (M = Cu, Ag, and Au) have also been studied recently [35], and the upper limits of the binding energies of the M^+–pyridine complexes have been obtained from the threshold of the photodissociative CT fragments. In this paper, we report on the photodissociation of the Mg^+–pyridine complex. The present study consists of mass selective photodissociation in a broad wavelength region of 240–440 nm and ab initio calculation of the relevant parent structure and its transition energies. The photodissociative CT reaction channel, as well as the non-reactive channel has been identified. The possible CT reaction mechanism is discussed.

2. Experiments and calculations

2.1. Experiments

The experimental setup has been described previously [23,24]. Briefly, a pulsed valve was utilized to generate clusters of pyridine by supersonic expansion of helium seeded with the pyridine vapor through a 0.5 mm diameter orifice. The backing pressure of helium was ~10 psi. The second harmonic (532 nm) of a Nd:YAG laser (~40 mJ/pulse) was weakly focused on a ~1 mm diameter spot of a magnesium disk. The laser-generated species, including the metal cations, traversed the supersonic jet stream perpendicularly. The intersection point was 2 cm from the magnesium disk and 1.5 cm from the nozzle exit. The nascent clusters and complexes traveled 14 cm down to the extraction region of the reflectron time-of-flight mass spectrometer (RTOFMS). The cation–molecule complexes were accelerated vertically by a high voltage pulse in a two-stage extractor. All the cluster cations were reflected by the reflectron and finally detected by a dual-plate micro-channel plate detector (MCP). For photodissociation experiments, a two-plate mass gate equipped with a high-voltage pulse-generator was used to select the desired cluster cations. The mass-selected cluster cations were irradiated with a collimated beam of a dye laser pumped by an excimer laser at the turn-around region of the reflectron. Fundamental outputs of the dyes including P-terphenyl, DMQ, BBQ, Stilbene 1, Coumarin 460 and second harmonic outputs of DCM, Kiton Red, Coumarin 540 A, Coumarin 503, and Coumarin 480 were used to cover the spectral region between 240 and 440 nm with reasonable wavelength overlaps. The photolysis laser fluence was kept low (<1 mJ/cm^2) to avoid multiphoton processes. The parent and nascent daughter cations were re-accelerated by the reflectron electric fields and detected by the MCP detector.

2.2. Calculations

The ground-state geometry of the Mg^+–pyridine complex was fully optimized at the B3LYP/6-31+G** level by using the GAUSSIAN 98 package. Two starting structures of the Mg^+–pyridine complex were attempted in our calculation: one was with Mg^+ bonded to the nitrogen atom at the side of the pyridine ring, and the other was with Mg^+ positioned above the pyridine ring. The binding energy of the complex was calculated from the difference between the total energy of the complex in its optimized ground-state geometry, E (Mg^+–pyridine), and the total energies of Mg^+ and pyridine as separated entities, E (Mg^+) + E (pyridine). In order to obtain the reaction energy of the CT, the products were also fully optimized at the same level. On the basis of the computational result for the ground state, vertical excitation energies to the low-lying excited states of the cation–molecule complex were calculated using a less extended configuration interaction (CI) referred to as the CI-single (CIS) approach.

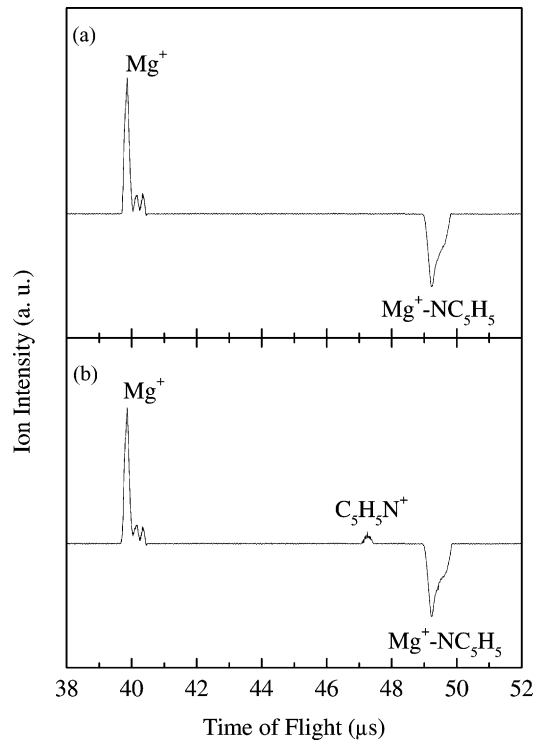

Fig. 1. Photodissociation difference mass spectra of Mg^+–pyridine at (a) 360 nm and (b) 247 nm.

3. Results and discussion

3.1. Photodissociation spectra of Mg^+–pyridine

After being produced, the Mg^+–NC_5H_5 complex was mass-selected and subjected to photodissociation at the turning point of the reflectron region. The photodissociation difference mass spectra of the complex at 360 nm (a) and 247 nm (b) are shown in Fig. 1 and are obtained by subtracting collected data taken with and without the photodissociation laser on. Thus, the negatively oriented peaks indicate the disappearance of the parent complex, and the positively oriented peaks correspond to the appearance of daughter ions. The photodissociation wavelengths fall respectively into the typical red-shifted and blue-shifted spectral bands with respect to the atomic transition of Mg^+ ($3^2P \leftarrow 3^2S$). These bands correspond to the promotion of the 3s valence electron of Mg^+ to the $3p_{x,y}$ and $3p_z$ orbitals, respectively. Judging from the photodissociation mass spectra in Fig. 1, Mg^+ from the photodissociation of Mg^+–pyridine seems to persist in the entire spectral region we studied (240–440 nm), whereas $C_5H_5N^+$ is only yielded in the higher energy spectral region. It is believed that the positive charge is localized on the Mg atom in the ground state of the complex because Mg has a lower ionization potential (7.65 eV) [36] than pyridine (9.26 eV) [37,38]. Therefore, the photodissociative reaction induced two channel products: a non-reactive channel product Mg^+ and a CT reactive channel product $C_5H_5N^+$ as shown in Fig. 1.

Fig. 2 shows the action spectrum of Mg^+–pyridine in the wavelength range of 240–440 nm, in which the total photofragment intensity is used. The dotted line at 280 nm represents the position of the $3^2P \leftarrow 3^2S$ atomic transition of Mg^+ [36]. The experimental action spectrum of the complex consists of three

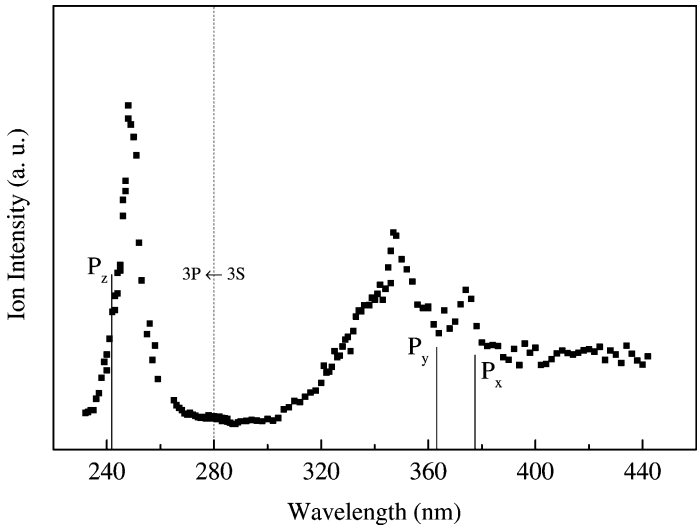

Fig. 2. Action spectrum of Mg^+–pyridine. The vertical axis represents the total photofragment ion yield. The dotted line indicates the atomic transition of Mg^+ ($^2P \leftarrow {}^2S$), and the solid lines show the calculated excitation energies and the oscillator strengths.

continuous structureless bands with an almost symmetrical feature. One of which (peak: ~248 nm) is situated in the blue-shifted spectral region with respect to the $3^2P \leftarrow 3^2S$ atomic transition of Mg^+, and the other two (peaks: ~347 and ~374 nm) are positioned in the red-shifted spectral region. The starting positions of these bands can be determined to be ~265, ~356, and ~380 nm, respectively, by taking the obvious rises of their longer wavelength sides as the starting positions. As will be discussed in the following sections, the observed bands in the action spectrum are from the splittings of the $3^2P \leftarrow 3^2S$ Mg^+ atomic transition. The reason for that is that the alignments of the three 3p orbitals in the excited states of Mg^+ with respect to the pyridine ligand are different, which causes the red-shifts (for 3^2P_x- and 3^2P_y-type states) and blue-shift (for 3^2P_z-type state) from the atomic transition in the spectrum. The symmetrical feature of the bands suggests that the three (3P-type) excited states all have a structure change with respect to the ground (3S-type) state.

Fig. 3 gives the relative yield of $C_5H_5N^+$ (I ($C_5H_5N^+$)/I (Mg^+)) as a function of laser wavelength. The CT product $C_5H_5N^+$ is only observed when the laser wavelength is within the range of 240–249 nm. The relative yield of $C_5H_5N^+$ is monotonously increased from ~0.02 to ~0.1 with the shortening of laser wavelength, which indicates that the CT channel is in competition with the non-reactive product channel near the threshold region. The reaction threshold seems to be set at ~249 nm. While the shortening of laser wavelength makes the relative yield of $C_5H_5N^+$ increase, the CT product cannot be observed when the laser wavelength is shorter than 240 nm. This may be due to the low excitation efficiency of the state in the spectral range as shown in Fig. 2 and the low laser efficiency of the dye.

3.2. Ab initio calculations

Theoretical ground-state structures for the pyridine molecule, pyridine cation, and Mg^+–pyridine complex were calculated as described before. The calculated structures of theirs are listed in Table 1. Also listed is that of pyridine optimized at the MP2(full)/6-31G* level [34] for comparison. It is obvious that the optimized structure of pyridine at the B3LYP/6-31+G** level is in good agreement with that at the MP2(full)/6-31G* level. The energies of alkali metal ion (Li^+, Na^+, and K^+) binding to

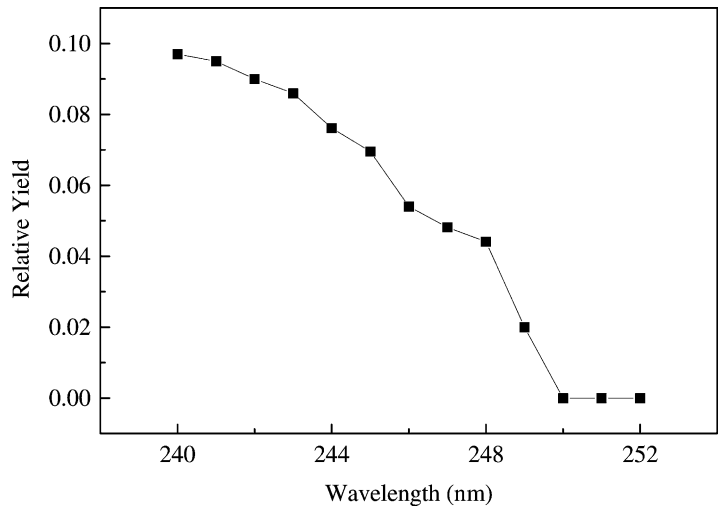

Fig. 3. Relative yield of pyridine ion (I ($C_5H_5N^+$)/(I (Mg^+)) as a function of laser wavelength.

Table 1
B3LYP/6-31+G** geometry optimized structures of neutral, ionized, and magnesium metalated pyridines

Parameters[a]	Species		
	Pyridine[b]	Pyridine cation	Mg^+–pyridine
Bond length (Å)			
1–2	1.341 (1.344)	1.314	1.354
2–3	1.397 (1.394)	1.407	1.390
3–4	1.396 (1.393)	1.397	1.397
4–5	1.396 (1.393)	1.397	1.397
5–6	1.397 (1.394)	1.407	1.390
6–1	1.341 (1.344)	1.314	1.354
1-Mg			2.133
2-H	1.088 (1.088)	1.087	1.088
3-H	1.086 (1.086)	1.086	1.084
4-H	1.086 (1.087)	1.086	1.086
5-H	1.086 (1.086)	1.086	1.084
6-H	1.088 (1.088)	1.087	1.088
Bond angle (°)			
123	123.6 (123.8)	114.3	122.4
234	118.5 (118.7)	118.9	118.8
345	118.5 (118.4)	121.0	119.1
456	118.5 (118.7)	118.9	118.8
561	123.6 (123.8)	114.3	122.4
612	117.2 (116.8)	132.5	118.5
Mg12			120.7
H23	120.4 (120.5)	125.3	120.7
H34	121.3 (121.2)	122.8	121.4
H45	120.6 (120.8)	119.5	120.5
H56	120.2 (120.2)	118.3	119.8
H61	115.8 (115.7)	120.4	116.9

[a] The number denotes C or N atom, where 1 is N atom.
[b] The parameters for the MP2(full)/6-31G* geometry optimized structure [34] are given in parentheses.

azine (pyridine, pyridazine, pyrimidine, pyrazine, and 1,3,5-triazine) calculated at the MP2(full)/6-31+G(2d, 2p) level using MP2(full)/6-31G* optimized geometries agree well with the GIBMS experimental results [34]. Furthermore, the agreement between the binding energy of Mg^+–pyridine calculated at the B3LYP/6-31+G** level (200.7 kJ/mol or 2.08 eV) and that determined experimentally (200.0 (6.4) kJ/mol) [33] is very satisfactory. All these facts validate our theoretical approach to the electronic and geometric structure of the complex.

While two different starting structures were tried in the optimization, only the one with Mg^+ bound to the N atom of the molecule possessing a C_{2v} symmetry with Mg on the C_2 axis of the complex (shown in Fig. 4 and Table 1) could be optimized at the B3LYP/6-31+G** level. For the complex with Mg^+ bound to the π cloud of pyridine, no local minimum could be found. The situation is in contrast to Au^+–pyridine [35c], where one isomeric structure possessing a C_1 symmetry with the Au atom resided over the C_1–C_2 bond and slightly shifted outside the perimeter of the aromatic ring is also optimized. This may be due to the relativistic effects in the gold atom resulting in increased covalent interaction between the gold metal and the ligand [35c]. However, the calculated structure is remarkably consistent with those complexes consisting of pyridine and most metal cations, such as Li^+, Na^+, K^+, Cu^+, Ag^+, Al^+, Sc^+, and Fe^+, etc. [33–35] and that of the Mg^+–pyridine complex optimized at a lower level of theory (B3LYP/6-31G(d, p)) [33]. Unfortunately, this level of theory is insufficient to obtain the accurate energetics for the system, since the agreement between the binding energy of the complex calculated at the B3LYP/6-31G(d, p) level and that determined experimentally (GIBMS) is poor [33].

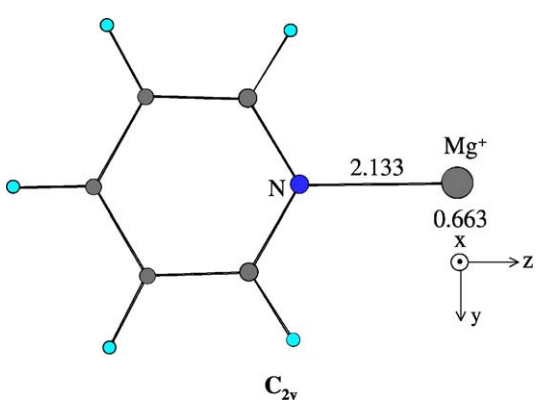

Fig. 4. Optimized ground-state structure of the Mg^+–pyridine complex at the B3LYP/6-31+G** level.

Pyridine, an azabenzene, can be treated either as a π-type ligand (similar to benzene) or as a σ-donor-type ligand because of the lone pair electrons on the nitrogen atom (similar to amine). The calculated result that Mg^+ prefers to be bound to the nitrogen atom rather than the π cloud of the aromatic ring of pyridine indicates that the interaction of Mg^+ with the lone pair electrons on N is indeed stronger than that with the π cloud. This can be appreciated from the binding energies of Mg^+–benzene (∼35.5 kcal/mol) [24] and Mg^+–amine (∼44 kcal/mol) [28,29]. For the Mg^+–amine complex [28,29], in addition to electrostatic interaction, covalent interaction plays an important part in the binding between Mg^+ and amine due to the σ-donor of the N atom in amine. Since the Mg^+–NC_5H_5 complex takes the structure as shown in Fig. 4, the covalent interaction should also be an important aspect for the complex binding.

In contrast to the Mg^+–amine complex, where only the σ donation interaction from the N lone pair electrons is involved in the covalent interaction [28,29], there are two types of covalent interactions participating in the Mg^+–N bond of Mg^+–NC_5H_5, e.g., a σ donation interaction from the pyridine $11A_1$ orbital (essentially the N lone pair) to the sp_z hybridized orbital of Mg^+ and a π donation interaction from the $2B_1$ π bonding orbital (essentially the delocalized π orbital on the aromatic ring) to the $3p_x$ orbital of Mg^+ (see Fig. 4). Therefore, it is expected that Mg^+–NC_5H_5 should have a stronger bond. The result is consistent with the binding energy calculated theoretically (2.08 eV or 48 kcal/mol) or determined experimentally (2.07 eV or 200.0 (6.4) kJ/mol) [33], which is larger than those of all the Mg^+–amine complexes studied by our group [28,29]. Correspondingly, the calculated bond length (2.133 Å) of Mg^+–NC_5H_5 is shorter than

those of all the Mg^+–amine complexes calculated at the same level [28,29]. The electron donations reduce the calculated total atomic charge on Mg^+ in the Mg^+–pyridine complex to 0.663. On the other hand, the large dipole moment (2.22 D) [35a] and polarizability (9.51 $Å^3$) [39] of pyridine may also enhance the electrostatic interaction between Mg^+ and the ligand.

3.3. Assignments of the action spectrum

The vertical excitation energies and the corresponding oscillator strengths of the complex are calculated at the CIS/6-31+G** level using the optimized geometry of its ground state obtained before. It must be pointed out that CIS is comparable to Hartree–Fock theory for ground-state systems in that it is qualitatively accurate if not always highly quantitatively predictive, since the CIS is described as an adequate zeroth-order treatment for many of the excited states of molecules [40]. A number of studies have shown the reliability of the CIS method for this type of complex or at least this calculation can satisfy our need to have a correct estimate on the general trends of the properties in question [3,24,28].

The calculated absorption spectrum is depicted in Fig. 2 as vertical solid lines. Except for the three transitions (3P-type) depicted in the figure, there are still three additional excited states (their vertical excitation energies are 334.0 nm or 3.71 eV, 295.9 nm or 4.20 eV, and 256.0 nm or 4.84 eV, respectively) located in the experimental spectral region. However, these other states have approximately zero oscillator strengths and thus are not shown. Fig. 2 clearly shows that the calculated spectrum is in agreement with the experimental spectrum in some respects, which suggests that only the three 3P-type states may be excited by the laser photon throughout the whole wavelength range.

In order to comprehend the spectrum of the complex, Fig. 5 shows the calculated vertical transitions of the complex and possible correlative separated asymptotes. Also shown are the schematic interaction diagrams of the $3P_{x,y,z}$ states of the complex. As shown in Fig. 5, in addition to the 3S ($^2A_1$) and $3P_x$ ($^2B_2$), $3P_y$ ($^2B_1$), $3P_z$ ($^2A_1$) states of the complex, represented as solid lines, correlated with the Mg^+ (3S)+C_5H_5N ($\tilde{X}$) and Mg^+ (3P)+C_5H_5N ($\tilde{X}$), asymptotes, respectively, the three states, shown as dashed lines, may be a CT state ($^2A_1$) corresponding to Mg^+ (3S)+$C_5H_5N^+$ ($\tilde{X}$) and two solvated molecular states possibly correlated to Mg^+ (3S)+C_5H_5N ($\tilde{A}$) (287 nm, $n \rightarrow \pi^*$ transition in pyridine [38]) and Mg^+ (3S)+C_5H_5N ($\tilde{C}$) (200 nm, $\pi \rightarrow \pi^*$ transition in pyridine [38]) asymptotes. The latter three states cannot be directly populated with the laser photon due to near zero calculated oscillator strengths. As will be discussed below, the fact that the CT state has a larger structure change with respect to the ground state may be one of the reasons that it has a close to zero oscillator strength. The solvated molecular transition moments and the CT transition moment are relatively small. This not only simplifies the assignments of the photodissociation action spectrum shown in Fig. 2, but also helps us to understand the CT reaction mechanism.

The action spectrum shown in Fig. 2 can be explained using the coordinate designation in Fig. 4 and schematic interaction diagrams in Fig. 5. In the excited states of 3^2P_x ($^2B_2$ in C_{2v}) and 3^2P_y ($^2B_1$ in C_{2v}) of Mg^+–pyridine, the two $3p_{x,y}$ orbitals of Mg^+ are perpendicular to the Mg^+–N bond, the electron density along the Mg^+–N bond is decreased, which reduces the electron repulsion. As a result, the static electric interaction between the metal cation and the lone pair electrons of the N atom is increased, and the binding energies of the excited states are both larger than that of the ground state. Therefore, the excitations of the $3^2P_{x,y}$-type states of the complex must be red-shifted from the Mg^+ atomic transition. The $3p_x$ orbital of Mg^+ is perpendicular to the pyridine ring plane, and parallels with the delocalized π orbital on the aromatic ring. As a result, the π bond interaction may be arisen upon the excitation of the $3P_x$-type state, which further lowers the energy of the state, giving rise to the largest red-shift as we observed. We, therefore, ascribe the two peaks at 374 and 347 nm in the action spectrum of Mg^+–NC_5H_5 to the vertical excitations of 3^2P_x (1^2B_2) and 3^2P_y (1^2B_1), respectively (the calculated values are 377.5 and 363.2 nm, respectively).

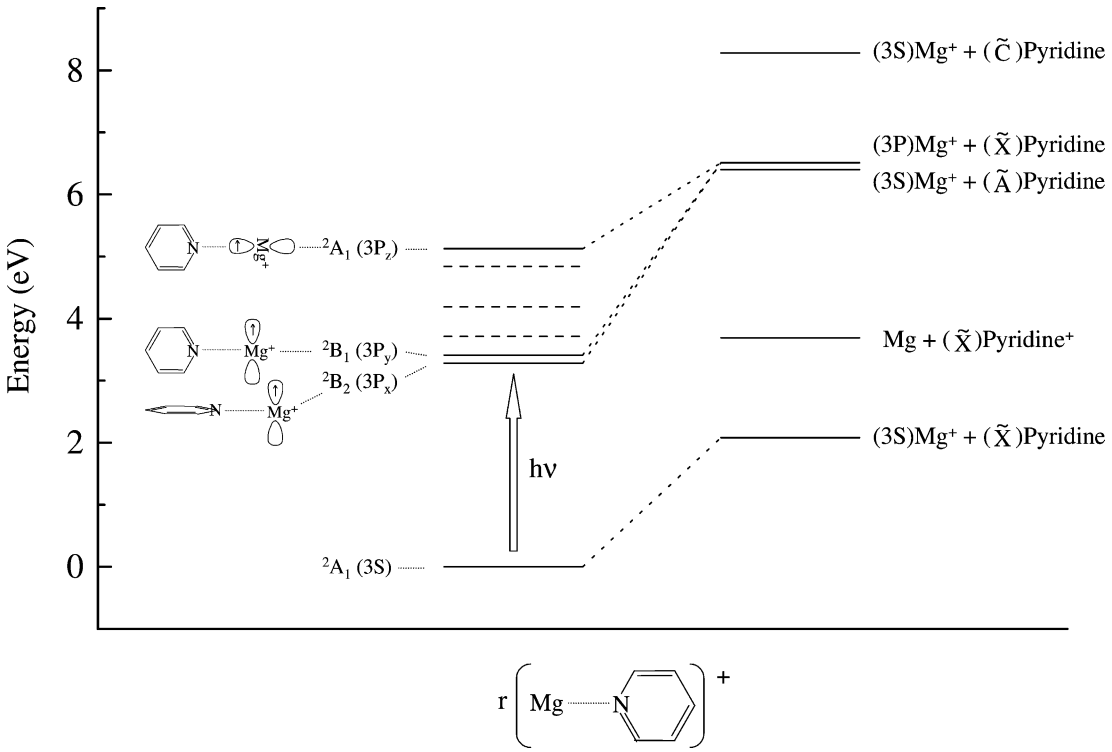

Fig. 5. Calculated energy levels of the Mg^+–pyridine complex and the possible asymptotes corresponding to Mg^+ (or Mg) and pyridine molecule (or cation). Also shown are the schematic interaction diagrams for the $3P_{x,y,z}$ states of the complex. The energies of the asymptotes are evaluated using the thermodynamic data taken from [33,36–38].

Although a good agreement between the excitation energy calculated theoretically and that determined experimentally exists in the 3^2P_x (1^2B_2) state, a larger difference between the two respects is appeared in the 3^2P_y (1^2B_1) state. The situation may be due to the qualitative accurateness of the CIS method as mentioned before [40]. However, to some extent the agreement between the theory and the experiment is good.

Since the $3P_{x,y}$-type states both have stronger Mg^+–pyridine bindings than the ground state, the Mg^+–N bond lengths of theirs should be shorter than that of the ground state. Thus, vertical transitions may excite the complex to the attraction parts of the $3P_{x,y}$ potential energy surfaces. This is consistent with the symmetrical feature of the bands relevant to the states shown in Fig. 2. The vertical excitations of the $3P_{x,y}$-type states are expected to be positioned at the peaks (374 and 347 nm) of both the red-shifted bands in the action spectrum due to the Frank–Condon integrations. The adiabatic transitions of the states may be situated close to the starting positions of the bands (380 nm or 3.26 eV and 356 nm or 3.48 eV for $3P_x$- and $3P_y$-type states, respectively). Taking the later two values as references, the binding energies of the $3P_x$ (1^2B_2) and $3P_y$ (1^2B_1) states can be evaluated to be 3.24 and 3.02 eV, respectively, by using simple energy cycle, where both the ground-state binding energy (2.07 eV) of Mg^+–pyridine and $3^2P \leftarrow 3^2S$ Mg^+ atomic transition (4.43 eV or 280 nm) which are needed in the evaluation were also determined experimentally [33,36]. Although the adiabatic transition of the lowest excited state ($3P_x$) of the complex is located at ~380 nm, the action spectrum shows a long tail till ~440 nm (see Fig. 2). As a possible explanation, the complexes from our pick-up source may have an internal energy of a fraction of an electron volt [28].

In the blue-shifted spectral region with respect to the $3^2P \leftarrow 3^2S$ atomic transition of Mg^+, the excitation is of a 3^2P_z-type, corresponding to a $^2A_1$ excited state. In this state, the occupied $3p_z$ orbital is aligned along the Mg^+–N bond axis (see Fig. 5), hence increases the direct repulsion between the $3p_z$ electron and the nitrogen lone pair electrons, which raises the energy of this excited state. Correspondingly, the binding energy of the excited state is smaller than that of the ground state, and the absorption of the 3^2P_z-type state of the complex must be blue-shifted from the Mg^+ atomic transition. Thus, we ascribe the peak at 248 nm in the action spectrum of Mg^+–NC_5H_5 to the vertical transition of the $^2A_1$ state (the calculated value is 241.9 nm). The fact that $3P_z$-type state has a weaker Mg^+–pyridine binding than the ground state makes the Mg^+–N bond lengths of the excited state longer. The complex can be excited to the repulsion part of the $3P_z$ potential energy surface by the laser photon, and the symmetrical band feature as shown in Fig. 2 is expected. Using the same way as for the $3^2P_{x,y}$-type states, the binding energy of the 3^2P_z-type state can be estimated to be 1.82 eV by using the starting position (265 nm or 4.68 eV) as the adiabatic transition of the state.

3.4. Dynamics of the photoinduced reactions

3.4.1. Non-reactive evaporation

As shown in Fig. 1, a main photodissociation channel leading to the formation of Mg^+ by non-reactive evaporation is open after the Mg^+–NC_5H_5 complex absorbs one photon in the whole spectral region. As discussed before, the Mg^+–NC_5H_5 complex is first pumped to a 3P-type state, suggesting that there are possibly two pathways for the producing of the non-reactive channel photofragment Mg^+, e.g., direct dissociation and pre-dissociation. In the first case, the reaction occurs along the excited state potential energy surface of the complex, which has been found in the case of the photodissociation spectroscopy of MgD_2^+ in the 2^2A_1 repulsive state [17]. The reason for the situation is that Mg^+H_2 is weakly bound in the 1^2A_1 ground state in C_{2v} geometry with D_e = 0.095 eV. However, for a strongly bound complex in the ground state such as Mg^+–NC_5H_5 (D_e = 2.07 eV from experiment [33] or 2.08 eV from calculation), this situation is always energy deficient. The minimum energy required for the direct dissociation can be calculated by simply adding the binding energy of the ground state of the complex and the excitation energy of the Mg^+ $3P \leftarrow 3S$ atomic transition (280 nm or 4.43 eV [36]). The evaluation gives the threshold energy for the direct dissociation to be ~6.5 eV for Mg^+–NC_5H_5, which is much higher than even the highest laser photon energy we used. Therefore, the non-reactive product Mg^+ is probably the result of pre-dissociation, which involves internal conversion from the original excited state to the ground state. This type of *E–V* quenching mechanism has been discussed extensively in the scientific literature [2,12–15,26,28,29].

3.4.2. Charge transfer reaction

It can be seen from Figs. 1 and 3, the minor CT product $C_5H_5N^+$ is observed when the laser wavelength is shorter than ~249 nm. The laser fluence dependence of this fragment makes us believe that the formation of the product from the photodissociation of Mg^+–pyridine is a single-photon process. On the other hand, referring to the thermodynamic data obtained from the scientific literature (the ionization potentials: Mg (7.65 eV) [36] and pyridine (9.26 eV) [37,38], the binding energy: Mg^+–pyridine (2.07 eV) [33]), we can estimate the threshold energy for the reaction to be 3.69 eV or 336 nm (the calculated value is 3.43 eV or 362 nm). This indicates that the energy of a photon is sufficient to start the reaction in the wavelength region and the single-photon process is possible.

CT is often found in organometallic and transition-metal chemistry, and it is well-known in condensed-phase metal complexes [41–43]. Photodissocative CT reaction in gas-phase metal cation–molecule complex systems was first reported by Duncan's group [8,9]. Photodissociative CT reaction provides a new route not only for the determination of metal cation–molecular dissociation energy, but also for the understanding of CT reaction in condensed-phase metal complexes

[8,9,35]. So far many photodissociative CT reactions have been reported in metal cation–molecule complexes [2,8,9,28,29,35]. CT in pyridine and metal cation systems has attracted widespread attention [35], since pyridine can be considered as a model in the study of biological system [30–35].

On the whole, two types of CT reactions may be involved in the photodissociation of a metal cation–molecule complex: one is direct photodissociative CT, and the other is predissociative CT. Fig. 6 (a) and (b) show the schematic diagrams of the two situations. As shown in Fig. 6a, for the direct photodissociative CT, the CT state is directly populated by a photon, followed by the dissociation which takes place on the CT potential energy surface giving exclusively rise to a metal atom and a molecule cation. Such a reaction has been observed in some metal cation–molecule complexes, such as M^+–benzene (M = Ag, Cu, etc.) and Ag^+–toluene, where only molecule cations were exclusively produced [8,9]. One fascinating aspect of photoinduced CT reaction is the determination of the upper limit of the ground-state binding energy of the metal cation–molecule complex (D_0), which can be estimated by the subtraction of the ionization potential difference of the molecule and the metal atom from the measured threshold energy of the CT [8,9,35]:

$$D_0 \leq h\nu_{CV} - \Delta IP \quad (1)$$

To the direct photodissociative CT, the difference between the upper limit estimated using (1) and the real value of the binding energy is determined by the position of the electronic transition with respect to the asymptote of the CT state (see Fig. 6a), thus a relatively small difference is usually obtained [8,9].

For the predissociative CT reaction (see Fig. 6b), however, except for the two states (G and CT), another excited electronic state (E) is also involved. Here the photon excites the complex to the excited state (E)

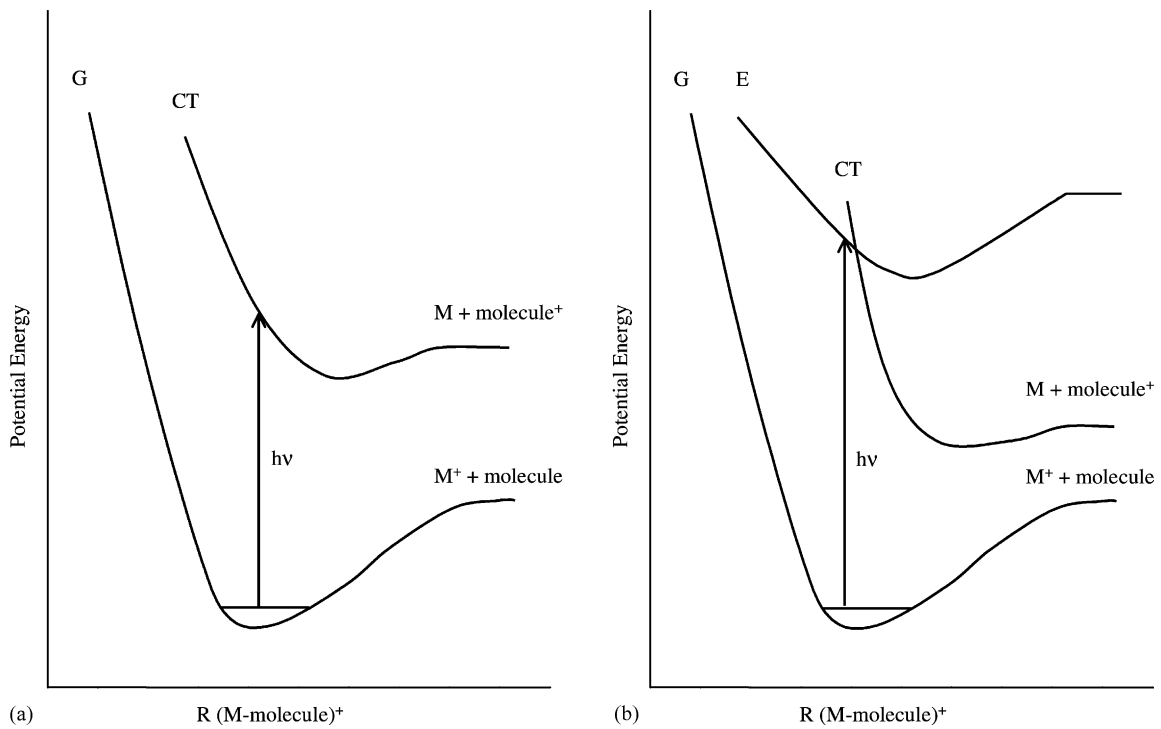

Fig. 6. Schematic potential energy diagram showing the photodissociative CT mechanisms of metal cation–molecule complex: (a) direct photodissociative CT and (b) predissociative CT.

instead of the CT state first, subsequently followed by an electronic curve crossing to the CT state and dissociating on the CT state yielding a metal atom and a molecular cation. Many of the CT reactions are classified as this type [28,29,44]. In this case, the crossing point of the two states (E and CT in Fig. 6b) usually determines the difference between the upper limit obtained using (1) and the real value of the ground-state binding energy of the complex. Therefore, sometimes a large difference can be introduced [2].

As shown in Figs. 2 and 5 and discussed before, for the Mg^+–pyridine complex, the stronger 3P ← 3S transitions of the solvated Mg^+ chromophore make the excitations of the solvated pyridine chromophore (such as $\pi^* \leftarrow n_N$ and $\pi^* \leftarrow \pi$ [38]) and that of the CT state by the photon in the same spectral region impossible. In order to clarify the viewpoint, Fig. 7 shows the measured action spectrum of the pyridine cation. Also shown is that of the total ion for comparison. The pyridine cation has a nearly similar spectral feature to the total ion and especially they have a common peak (at ~248 nm). The fact indicates that only one state is excited by the laser photon in the spectral region. Furthermore, the monotonous increase of the relative yield of $C_5H_5N^+$ with the shortening of laser wavelength as shown in Fig. 3 also suggests that the CT and non-reactive product channels are the competing processes from an initially photo-populated state. Since Mg^+ rather than the pyridine cation is the main product (see Figs. 1b and 3), the photon should excite the 3P-type state rather than the CT state. We thus think the CT reaction from the photodissociation of Mg^+–pyridine may be ascribed to a predissociative CT process (as Fig. 6b). That is, the complex is excited to a 3P state by one photon, and then crosses to the CT state giving rise to a Mg atom and a pyridine cation in their ground electronic states.

The $3P_{x,y}$ states of the complex are lower than the CT state (one of the three dash lines) in the vertical transition region, whereas the situation of their asymptotes is reversed (see Fig. 5). Therefore, it is expected that the $3P_{x,y}$ states should cross with the CT state at some points. However, the crossing probabilities from the $3P_{x,y}$ states (B_2 and B_1 symmetries in C_{2v}, respectively) to the CT state (A_1 symmetry in C_{2v}) are expected to be very small, since the two crossing states have different symmetries. This is consistent with the photodissociation difference mass spectrum shown in Fig. 1a, where no CT product is observed in the spectral region.

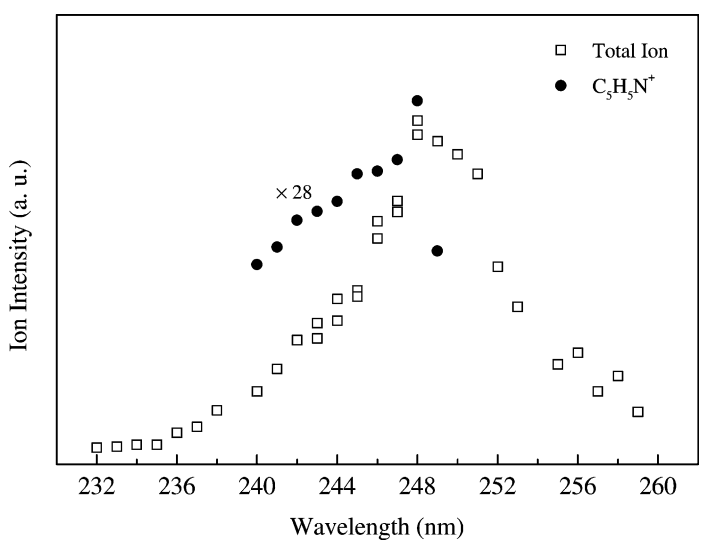

Fig. 7. Action spectrum of the CT product $C_5H_5N^+$ from the photodissociation of Mg^+–pyridine. Also depicted is that of the total ion for comparison.

For the $3P_z$-type state, the energy of the state is higher than that of the CT state either in the region of the vertical transition or that of their asymptotes (see Fig. 5), but the probability exists to cross at the repulsion part of the $3P_z$ potential energy surface. As the two states have the same A_1 symmetry in the C_{2v} group, the internal conversion probability from the photo-excited state $3P_z$ to the CT state is expected to be larger than that from the $3P_{x,y}$ states. On the other hand, judging from the complex structure shown in Fig. 4, we also imagine that the electron on the $3p_z$ orbital (along the Mg–N bond) can exert a large influence on the lone pair electrons of the nitrogen atom giving rise to the ionization of the pyridine molecule. The fact that the angle of the C–N–C is increased as large as ∼13% (612 in Table 1) upon the ionization of pyridine suggests the ionized electron is really from the lone pair of N rather than from the π orbital of the aromatic ring. Furthermore, the energy of the crossing point is much higher than that of the threshold of the CT reaction as given above (336 nm or 3.69 eV from experimental thermodynamic data or 362 nm or 3.43 eV from the calculation). As a result, the CT product may be observed in this spectral region, which is consistent with the experimental results we obtained (see Figs. 1b, 3, and 7). Although the photon energy in the entire $3P_z$ excited region (240–260 nm or 5.17–4.77 eV) is much higher than the threshold energy of the CT reaction, we only observed the CT product when the laser wavelength is shorter than 249 nm or ∼5 eV. Thus, the crossing point of the two states may be near this position. In other words, if we take 249 nm as the threshold of the CT reaction, the upper limit of the binding energy of Mg^+–pyridine can be placed on 3.37 eV using (1), which is much higher than the measured (2.07 eV) [33] or calculated (2.08 eV) value. A similar crossing has also been observed in the photodissociation of the complexes of Mg^+ with other N-containing molecules, such as methylamine [29] and ammonia [44].

The predissociative CT is favored in the $3P_z$ excited region, however, as shown in Figs. 1b, 3, and 7, it is still a minor process. The reason is that another *E–V* quenching from the $3P_z$ state to the highly vibrational excited ground state (3S) giving rise to the non-reactive product Mg^+ competes with the crossing to the CT state. In the CT state, positive charge is distributed on the molecule, and the metal atom is larger than the metal cation, which results in a longer M-ligand bond. The CT state should have a larger structure change relative to the ground state than the $3P_z$ state does. Therefore, although both the CT state and $3P_z$ state possess the same symmetry (A_1) as the 3S state, the larger structure change of the CT state may decrease the crossing probability from the $3P_z$ state to it. The *E–V* quenching from the $3P_z$ state to the ground electronic state (3S) is expected to be much stronger than that to the CT state, and the non-reactive channel product Mg^+ is the main product.

It is instructive to compare the photodissociation spectra of Mg^+–pyridine with those of Cu^+–pyridine (or Ag^+–pyridine, Au^+–pyridine) [35]. In the latter cases only the CT product pyridine cation was exclusively observed, which is much different from the experimental results shown in Fig. 1. The reason may be that in the cases of Cu^+–pyridine (or Ag^+–pyridine, Au^+–pyridine) the photon excited the solvated pyridine chromophore and the CT state of the complex [35]. A similar situation can also be found between Mg^+–benzene [9,24] and Ag^+–benzene (or Cu^+–benzene) [8,9].

4. Conclusion

Photodissociation spectroscopy of the Mg^+–NC_5H_5 complex has been studied. The non-reactive product Mg^+ is always observed for the complex at all laser wavelengths we studied, whereas the weak CT reactive channel product $C_5H_5N^+$ is only yielded in the higher energy spectral region. The action spectrum of the complex consists of three pronounced bands with an almost symmetrical feature. The bands are positioned in the red-shifted and blue-shifted spectral region with respect to the Mg^+ $3^2P \leftarrow 3^2S$ atomic transition. The optimized geometry of Mg^+–NC_5H_5 is characterized by the linkage of Mg^+ to the N atom of the molecule possessing a C_{2v} symmetry with Mg

on the C_2 axis of the complex. The vertical absorption spectrum of Mg^+–pyridine calculated using the optimized geometry of its ground state agrees qualitatively with the observed action spectrum. The result indicates that only the transitions of the solvated Mg^+ chromophore are involved in the experimental spectral region. The binding energies of the $3P_x$, $3P_y$, and $3P_z$ states are evaluated to be 3.24, 3.02, and 1.82 eV, respectively, from the photodissociation experiment. We use the predissociative CT mechanism to discuss the CT reaction observed in the spectral region of the $3P_z$ state. It is the photo-populated $3P_z$ state which crosses to the CT state giving rise to the CT product.

Acknowledgements

This work is supported by a RGC grant administered by the UGC of Hong Kong. W.Y.G. thanks F. Hegmann for his helpful discussion.

References

[1] S.S. Wesolowski, R.A. King, H.F. Schaefer III, M.A. Duncan, J. Chem. Phys. 113 (2000) 701.
[2] (a) P.D. Kleiber, J. Chen, Int. Rev. Phys. Chem. 17 (1998) 1; (b) J. Chen, Y.C. Wong, Y.C. Cheng, K. Montgomery, P.D. Kleiber, J. Chem. Phys. 108 (1998) 2285; (c) J. Chen, T.H. Wong, P.D. Kleiber, Chem. Phys. Lett. 279 (1997) 185.
[3] J.H. Holmes, P.D. Kleiber, D.A. Olsgaard, K.-H. Yang, J. Chem. Phys. 112 (2000) 6583.
[4] W.-Y. Lu, P.D. Kleiber, J. Chem. Phys. 114 (2001) 10288.
[5] (a) C.S. Yeh, J.S. Pilgrim, K.F. Willey, D.L. Robbins, M.A. Duncan, Int. Rev. Phys. Chem. 13 (1994) 231; (b) M.A. Duncan, Ann. Rev. Phys. Chem. 48 (1997) 69; (c) C.S. Yeh, K.F. Willey, D.L. Robbin, M.A. Duncan, Int. J. Mass Spectrom. Ion Process. 131 (1994) 307.
[6] J. Qian, A.J. Midley, S.G. Donnelly, J.I. Lee, J.M. Farrar, Chem. Phys. Lett. 244 (1995) 414.
[7] (a) C.S. Yeh, K.F. Willey, D.L. Robbins, M.A. Duncan, J. Phys. Chem. 96 (1992) 7833; (b) C.S. Yeh, K.F. Willey, D.L. Robbins, J.S. Pilgrim, M.A. Duncan, J. Chem. Phys. 98 (1993) 1867; (c) C.T. Scurlock, S.H. Pullins, M.A. Duncan, J. Chem. Phys. 105 (1997) 3579.
[8] K.F. Willey, P.Y. Cheng, M.B. Bishop, M.A. Duncan, J. Am. Chem. Soc. 113 (1991) 4721.
[9] K.F. Willey, C.S. Yeh, D.L. Robbins, M.A. Duncan, J. Phys. Chem. 96 (1992) 9106.
[10] D.C. Sperry, A.J. Midey, J.I. Lee, J. Qian, J.M. Farrar, J. Chem. Phys. 111 (1999) 8469.
[11] M. Sanekata, F. Misaizu, K. Fuke, S. Iwata, K. Hashimoto, J. Am. Chem. Soc. 117 (1995) 747.
[12] M. Sanekata, F. Misaizu, K. Fuke, J. Chem. Phys. 104 (1996) 9768.
[13] F. Misaizu, M. Sanekata, K. Fuke, J. Chem. Phys. 100 (1994) 1161.
[14] J. Chen, Y.C. Cheng, P.D. Kleiber, J. Chem. Phys. 106 (1997) 3884.
[15] Y.C. Cheng, J. Chen, L.N. Ding, T.H. Wong, P.D. Kleiber, D.-K. Liu, J. Chem. Phys. 104 (1996) 6452.
[16] J.I. Lee, D.C. Sperry, J.M. Farrar, J. Chem. Phys. 114 (2001) 6180.
[17] (a) L.N. Ding, M. Young, P.D. Kleiber, W.C. Stwalley, A.M. Lyyra, J. Phys. Chem. 97 (1993) 2181; (b) L.N. Ding, P.D. Kleiber, M.A. Young, W.C. Stwalley, A.M. Lyyra, Phys. Rev. A 48 (1993) 2024.
[18] C.W. Bauschlicher Jr., M. Sodupe, H. Partridge, J. Chem. Phys. 96 (1992) 4453.
[19] K.N. Kirschner, B. Ma, J.P. Bowen, M.A. Duncan, Chem. Phys. Lett. 295 (1998) 204.
[20] C.W. Bauschlicher Jr.,, H. Partridge, J. Phys. Chem. 95 (1991) 3946.
[21] C.W. Bauschlicher Jr., H. Partridge, Chem. Phys. Lett. 181 (1991) 129.
[22] H. Watanabe, S. Iwata, K. Hashimoto, F. Misaizu, K. Fuke, J. Am. Chem. Soc. 117 (1995) 755.
[23] (a) Y. Yang, Y.H. Hu, S.H. Yang, J. Phys. Chem. A 104 (2000) 8496; (b) X. Yang, Y.H. Hu, S.H. Yang, Chem. Phys. Lett. 322 (2000) 491; (c) X. Yang, H.C. Liu, S.H. Yang, J. Chem. Phys. 113 (2000) 3111.
[24] X. Yang, K.L. Gao, H.C. Liu, S.H. Yang, J. Chem. Phys. 112 (2000) 10236.
[25] H.C. Liu, C.S. Wang, W.Y. Guo, Y.D. Wu, S.H. Yang, J. Am. Chem. Soc. 124 (2002) 3794.
[26] W.Y. Guo, H.C. Liu, S.H. Yang, J. Chem. Phys. 116 (2002) 9690.
[27] H.C. Liu, W.Y. Guo, S.H. Yang, J. Chem. Phys. 115 (2001) 4612.
[28] W.Y. Guo, H.C. Liu, S.H. Yang, J. Chem. Phys. 116 (2002) 2896.
[29] W.Y. Guo, H.C. Liu, S.H. Yang, J. Chem. Phys. 117 (2002) 6061.
[30] F. Brody, P.R. Ruby, in: E. Klingsberg (Ed.), Heterocyclic Compounds, Pyridine and Derivatives, Part 1, Interscience Publishers, New York, 1960, p. 99.
[31] R.T. Coutts, A.F. Casy, in: R.A. Abramovitch (Ed.), Pyridine and Its Derivatives, Suppl., Part 4, John & Sons, New York, 1975, p. 445.
[32] T.L. Gilchrist, Heterocyclic Chemistry, 3rd ed., Longman Singapore Publisher Inc., Singapore, 1997, p. 125.
[33] M.T. Rodgers, J.R. Stanley, R. Amunugama, J. Am. Chem. Soc. 122 (2000) 10969.

[34] R. Amunugama, M.T. Rodgers, Int. J. Mass Spectrom. 195/196 (2000) 439.
[35] (a) Y.S. Yang, W.Y. Hsu, H.F. Lee, Y.C. Huang, C.S. Yeh, J. Phys. Chem. A 103 (1999) 11287;
(b) Y.S. Yang, C.S. Yeh, Chem. Phys. Lett. 305 (1999) 395;
(c) H.S. Hsu, F.W. Lin, C.C. Lai, P.H. Su, C.S. Yeh, N. J. Chem. 26 (2002) 481.
[36] D.R. Lide, CRC Handbook of Chemistry and Physics, 79th ed., CRC Press, Boca Raton, Boston, London, New York, Washington, DC, 1998–1999.
[37] E. Moore, Atomic Energy Levels, National Bureau of Standards, Washington, DC, 1971.
[38] G. Herzberg, Electronic Spectra and Electronic Structure of Polyatomic Molecules, Van Nostrand Reinhold, New York, 1966.
[39] J.F. Sanz, J. Anguiano, J. Vilarrasa, J. Comput. Chem. 9 (1988) 784.
[40] J.B. Foresman, Æ. Frish, Exploring Chemistry with Electronic Structure Methods, 2nd ed., Gaussian, Pittsburgh, 1996.
[41] R.A. Beyer, J.A. Vanderhoff, J. Chem. Phys. 65 (1976) 2313.
[42] (a) M.F. Jarrold, L. Misev, M.T. Bowers, J. Chem. Phys. 81 (1984) 4369;
(b) H.Y. Kim, C.H. Kuo, M.T. Bowers, J. Chem. Phys. 87 (1987) 2667.
[43] E.J. Bieske, A.M. Solvia, A. Friedman, J.P. Maier, J. Chem. Phys. 96 (1992) 7535.
[44] S. Yoshida, N. Okai, K. Fuke, Chem. Phys. Lett. 347 (2001) 93.